NAL TR-404T

UDC 519.28:
533.048.5

TECHNICAL REPORT OF NATIONAL AEROSPACE LABORATORY

TR-404T

Shear and Moment Response of the Airplane Wing to Nonstationary Turbulence

Yoshinori FUJIMORI

January 1975

NATIONAL AEROSPACE LABORATORY

CHŌFU, TOKYO, JAPAN

Shear and Moment Response of the Airplane Wing to Nonstationary Turbulence*

By Yoshinori FUJIMORI**

ABSTRACT

Response formulation of the shear force and bending moment of the airplane wing has been established in terms of evolutionary cross spectrum. Frequency distribution of the responses of arbitrary wing sections can be obtained at any time instant of our interest after the airplane enters the nonstationary atmospheric turbulence. Conventional stationary solutions are included in this analysis as the special case.

Contribution by the pitching motion is the highest to both shear and moment responses. The effect of the shear force to the stress level is negligibly smaller than that due to the bending moment.

When the envelope profile looks like a step function, mean square moment takes the maximum in the transient stage whose spectrum is dominated by rigid modes. But the spectrum at stationary state, where its mean square moment is lower than the transient maximum, shows both rigid and flexible motions. Therefore the search of the stationary solutions only is not adequate in view of ultimate strength and fatigue life of the airplane structure.

概　　要

上下方向の非定常大気乱流によって加振される航空機翼に生ずるせん断力，曲げモーメントを求める式を導き，結果を時間とともに変る変化スペクトル（Evolutionary Spectrum）で表示した。従来の定常的な解析は本法の特別な場合である。航空機の運動としては上下動，Pitching 主翼1次曲げの3自由度をとったが，この中で Pitching の寄与が一番大きい。スペクトルの結果から，過渡応答では剛体自由度が主であって，定常応答ではこれらの外に主翼曲げの自由度が入ってくることが分った。全応答のレベルを示す r.m.s. 値は考慮する非定常性にもよるが，過渡応答時に最大となるので，定常解だけを求める従来の解析は不十分である。

INTRODUCTION

Necessity to analyze the nonstationary structural responses has grown out of our broad experiences that various phenomena such as airplane motion in the gust, ground buildings' response under the earthquakes, overshoot of vibration amplitude in reciprocating or rotary machineries and so forth show mostly the nonstationary time-wise trend. Within the scope of aeronautical problems most flight records of the acceleration response in the turbulence are said to be of nonstationary random nature, and in the worst case a big airplane suffers structural catastrophe just after entering the turbulent field behind the high mountain even in the clear sky.

Data piled up for years by means of observations or experiment indicate to us how essential the transient vibration is from the view point of tolerable load as well as fatigue damage of the structure. Although the analysis of the airplane response to the atmospheric turbulence was tried as early as in 1930's and the advance in the stochastic technique gave impetus to the improvement of the analysis, our

* Received Octber 22, 1974.

** 2nd Airframe Division.

knowledge has in most cases remained in the stationary regime. Moreover since it was thought that the spectrum analysis of the time series is valid only for stationary processes, the progress of nonstationary analysis has been so limited in spite of its importance.

The first attempt was lately made by Howell and Lin[3] who analyzed the plunging mode response of the airplane to nonstationary atmospheric turbulence using evolutionary power spectra proposed by Priestley. As the original definition by Priestley pertains to the single-degree-of-freedom problems, Fujimori and Lin extended the concept to evolutionary cross spectra analysis of the response of multi-modal linear systems[1),2)], which is the up-to-date general method to obtain the nonstationary responses as well as the stationary ones. Various responses of our interests such as displacement, velocity and acceleration at a certain time instant are to be estimated in terms of evolutionary spectra and their mean square values. Those results emphasize quantitative anticipation of transient maximum responses and comparison between those and conventional stationary responses.

In this report the author intends to work out the procedure to calculate important responses such as the acting forces on the wing, shear force and bending moment of the airplane wing sections to nonstationary atmospheric turbulence. By making use of their practical values we are able to evaluate the stress or strain levels in the structure, which seems an indispensable task at the initial design phase of the all aircrafts. The numerical examples are carried out about the same model handled in the previous reports[1),2)].

PROBLEM STATEMENTS

We are considering the airplane as the multi-modal linear system whose motion is governed by[2)]

$$M_j \ddot{\xi}_j + \beta_j \dot{\xi}_j + M_j \omega_j^2 \xi_j = Q_j \qquad (1)$$

where

$M_j = \int \phi_j^2(x, y)\rho(x, y)dxdy$ = j-th generalized mass

$Q_j = \int \{ F^M(x, y, t) + F^G(x, y, t) \} \phi_j(x, y)dxdy$

= j-th generalized force

ξ_j = j-th generalized coordinate

ϕ_j = j-th mode eigen function

ρ_j = mass per unit area of the airplane wing

β_j = damping coefficient of j-th mode

ω_j = j-th circular natural frequency

Aerodynamic forces are simply assumed to be

$$F^M(x, y, t) = -\pi\rho_0 b\, z(x, y, t)/2 - \pi\rho_0 U \times \int_0^t \dot{z}(x, y, t_1)\,\phi(t-t_1)\,dt_1 \qquad (2)$$

$$F^G(x, y, t) = \pi\rho_0 U \int_0^t W(x-Ut_1, y)\,\dot{\psi}(t-t_1)\,dt_1 \qquad (3)$$

where $z(x, y, t) = \sum_j \phi_j(x, y)\,\xi_j(t)$ = Total response

$\phi(t)$ = Wagner's function

$\psi(t)$ = Küssner's function

b = A half of the reference chord length

U = Airplane forward velocity

$W(x-Ut, y)$ = Vertical gust velocity

ρ_0 = Air density

(x,y) are moving coordinates that have the origin at the gravity center of the airplane.

In writting Eq. (2) and (3) two-dimensional aerodynamic theory in incompressible flow (strip theory) is adopted. These aerodynamic forces are assumed to depend only on the local motion and local gust velocity. No claim is made of the accuracy when Eq. (2) and (3) are applied to a practical airplane geometry, but they appear to be reasonable assumptions for the purpose of the present study. We have shown the procedure to obtain the impulse response matrix of the system by making use of equations (1), (2) and (3) in the previous study[2]. The expressions of forces acting on the wing, shear and moment at the wing section of our interest will be derived about the wing configuration illustrated by Fig. 1. First the acting force on the wing at the coordinates (x,y) per unit area is given by

$$\begin{aligned} F(x, y, t) &= F^M + F^G - \rho_w \ddot{z} \\ &= \pi\rho_0 U \int_0^t W(x-U\tau, y)\,\dot{\psi}(t-\tau)\,d\tau \\ &\quad - \pi\rho_0 U \int_0^t \dot{z}(x, y, \tau)\,\phi(t-\tau)\,d\tau \\ &\quad - \pi\rho_0 b\,\dot{z}(x, y, t)/2 - \rho(x, y)\,\ddot{z}(x, y, t) \end{aligned} \qquad (4)$$

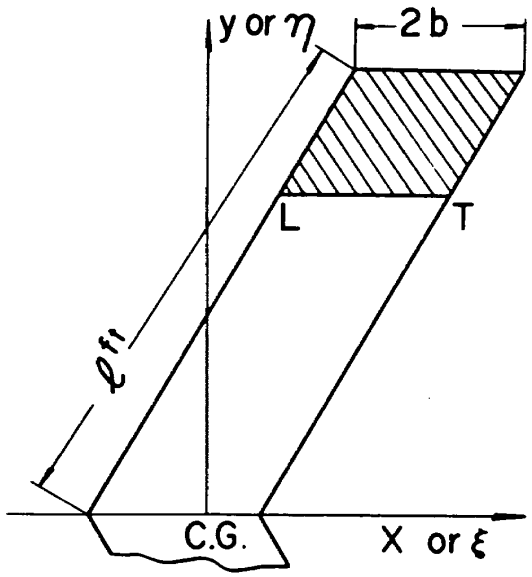

Fig. 1 Coordinates of the Swept-back Wing Configuration.

Putting $\hat{\rho}_{1,2}=\rho_w(x_{1,2}, y_{1,2})+\pi\rho_0 Ub/2$ and $\Pi=\pi\rho_0 U$ the expectation of the product of $F(x_1, y_1, t_1)$ and $F(x_2, y_2, t_2)$ can be written as

$$
\begin{aligned}
&E[F(x_1, y_1, t_1)F(x_2, y_2, t_2)]\\
&=\Pi^2\int_0^{t_1}\dot{\psi}(t_1-\tau_1)\,d\tau_1\\
&\times\int_0^{t_2}\dot{\psi}(t_2-\tau_2)\,d\tau_2\,E[W(x_1-U\tau_1, y_1)W(x_2-U\tau_2, y_2)]\\
&-\Pi^2\int_0^{t_1}\dot{\psi}(t_1-\tau_1)\,d\tau_1\\
&\times\int_0^{t_2}\phi(t_2-\tau_2)\,d\tau_2\,E[W(x_1-U\tau_1, y_1)\dot{z}(x_2, y_2, \tau_2)]\\
&-\Pi^2\int_0^{t_2}\dot{\psi}(t_2-\tau_2)\,d\tau_2\\
&\times\int_0^{t_1}\phi(t_1-\tau_1)\,d\tau_1\,E[\dot{z}(x_1, y_1, \tau_1)W(x_2-U\tau_2, y_2)]\\
&+\Pi^2\int_0^{t_1}\phi(t_1-\tau_1)\,d\tau_1\\
&\times\int_0^{t_2}\phi(t_2-\tau_2)\,d\tau_2\,E[\dot{z}(x_1, y_1, \tau_1)\dot{z}(x_2, y_2, \tau_2)]\\
&-\Pi\int_0^{t_1}\dot{\psi}(t_1-\tau_1)\,d\tau_1\,\hat{\rho}_2\,E[W(x_1-U\tau_1, y_1)\dot{z}(x_2, y_2, t_2)]\\
&-\Pi\int_0^{t_2}\dot{\psi}(t_2-\tau_2)\,d\tau_2\,\hat{\rho}_1\,E[\dot{z}(x_1, y_1, t_1)W(x_2-U\tau_2, y_2)]\\
&+\Pi\int_0^{t_1}\phi(t_1-\tau_1)\,d\tau_1\,\hat{\rho}_2\,E[\dot{z}(x_1, y_1, \tau_1)\dot{z}(x_2, y_2, t_2)]\\
&+\Pi\int_0^{t_2}\phi(t_2-\tau_2)\,d\tau_2\,\hat{\rho}_1\,E[\dot{z}(x_1, y_1, t_1)\dot{z}(x_2, y_2, \tau_2)]\\
&+\hat{\rho}_1\hat{\rho}_2\,E[\dot{z}(x_1, y_1, t_1)\dot{z}(x_2, y_2, t_2)] \qquad (5)
\end{aligned}
$$

The shear and moment at the wing section L-T can be obtained by integration of Eq. (5) within the hatched area (H. A) of Fig. 1, then we formulate the expectation of the product of the shear forces at (y_1, t_1) and (y_2, t_1) in the following.

$$
\begin{aligned}
&E[S(y_1, t_1)S(y_2, t_2)]\\
&=\iint_{H.A._1}d\xi_1\,d\eta_1\iint_{H.A._2}d\xi_2\,d\eta_2\,E[F(\xi_1, \eta_1, t_1)F(\xi_2, \eta_2, t_2)] \qquad (6)
\end{aligned}
$$

y_1 and y_2 indicate the distance from the wing root, t_1 and t_2 the corresponding time instants. For the bending moment we also have

$$
\begin{aligned}
&E[M(y_1, t_1)M(y_2, t_2)]\\
&=\iint_{H.A._1}d\xi_1\,d\eta_1\iint_{H.A._2}d\xi_2\,d\eta_2\,(\eta_1-y_1)(\eta_2-y_2)\\
&\times E[F(\xi_1, \eta_1, t_1)F(\xi_2, \eta_2, t_2)] \qquad (7)
\end{aligned}
$$

As is assumed in the previous work, the nonstationary gust velocity is factored into the product of a deterministic envelope function $C(x-Ut, y)$ and a stationary random gust velocity $G(x-Ut, y)$,

$$W(x-Ut, y)=C(x-Ut, y)\,G(x-Ut, y) \qquad (8)$$

Also we assumed

$$C(x-Ut, y)=C_0\{e^{-\alpha(Ut-x)}-e^{-\beta(Ut-x)}\} \qquad (9)$$

where C_0 is a normalizing constant and α, β are gust parameters with $0\leq\alpha<\beta$. Stationary part of the vertical gust G has the spectrum

$$\Phi(\xi, \eta, \omega)=\Phi_d(\omega)\,e^{-i\omega\xi/U} \qquad (10)$$

where $\xi=x_1-x_2$, $\eta=y_1-y_2$ and $\Phi_d(\omega)=$ Dryden's spectrum.

The final form of the force per unit area of the wing, shear and moment are given by

$$
\begin{Bmatrix}
E[F(x_1, y_1, t_1)F(x_2, y_2, t_2)]\\
E[S(y_1, t_1)S(y_2, t_2)]\\
E[M(y_1, t_1)M(y_2, t_2)]
\end{Bmatrix}
$$

$$= \int_{-\infty}^{+\infty} e^{i\omega(t_1-t_2)} \times \begin{Bmatrix} \Psi_F(x_1, y_1, t_1, x_2, y_2, t_2 ; \omega) \\ \Psi_S(y_1, t_1, y_2, t_2 ; \omega) \\ \Psi_M(y_1, t_1, y_2, t_2 ; \omega) \end{Bmatrix} d\omega \tag{11}$$

where $\Psi_{\{F,S,M\}} = \Psi_{\{F,S,M\},\alpha\alpha} - \Psi_{\{F,S,M\},\alpha\beta} - \Psi_{\{F,S,M\},\beta\alpha} + \Psi_{\{F,S,M\},\beta\beta}$ (12)

$$\begin{aligned}
\Psi_{\{F,S,M\},\alpha\beta} = C_0^2 \Phi_d(\omega) \Big[& {}_1T_{\{F,S,M\},\alpha\beta}(x_1, y_1, t_1; x_2, y_2, t_2; \omega) \\
& - \sum_k \sum_l \{ \Pi^3 \, {}_2T_{\{F,S,M\},\alpha\beta,kl}(x_1, y_1, t_1; x_2, y_2, t_2 ; \omega) \\
& + \Pi^3 \, {}_2T^*_{\{F,S,M\},\alpha\beta,kl}(x_2, y_2, t_2; x_1, y_1, t_1; \omega) \\
& + \Pi^2 \, {}_5T_{\{F,S,M\},\alpha\beta,kl}(x_1, y_1, t_1; x_2, y_2, t_2; \omega) \\
& + \Pi^2 \, {}_5T^*_{\{F,S,M\},\alpha\beta,kl}(x_2, y_2, t_2; x_1, y_1, t_1; \omega) \} \\
& + \sum_j \sum_k \sum_l \sum_m \{ \Pi^4 \, {}_4T_{\{F,S,M\},\alpha\beta,jklm}(x_1, y_1, t_1; x_2, y_2, t_2; \omega) \\
& + \Pi^2 \, {}_7T_{\{F,S,M\},\alpha\beta,jklm}(x_1, y_1, t_1; x_2, y_2, t_2; \omega) \\
& + \Pi^2 \, {}_7T^*_{\{F,S,M\},\alpha\beta,jklm}(x_2, y_2, t_2; x_1, y_1, t_1; \omega) \\
& + \Pi^2 \, {}_9T_{\{F,S,M\},\alpha\beta,jklm}(x_1, y_2, t_1; x_2, y_2, t_2; \omega) \} \Big]
\end{aligned} \tag{13}$$

The asterisk (*) indicates the conjugate.

$$\begin{aligned}
& {}_1T_{\{F,S,M\},\alpha\beta}(x_1, y_1, t_1; x_2, y_2, t_2, \omega) \\
& = N_\alpha(t_1, \omega) N^*_\beta(t_2, \omega) \{ A_{F,\alpha}(x_1, y_1, \omega) \\
& \times A^*_{F,\beta}(x_2, y_2, \omega), \; A_{S,\alpha}(y_1) A^*_{S,\beta}(y_2), \\
& A_{M,\alpha}(y_1) A^*_{M,\beta}(y_2) \}
\end{aligned} \tag{14}$$

$$\begin{aligned}
& {}_2T_{\{F,S,M\},\alpha\beta,kl}(x_1, y_1, t_1; x_2, y_2, t_2; \omega) \\
& = N_\alpha(t_1, \omega) \hat{M}^*_{kl,\beta}(t_2, \omega) R^*_{l,\beta}(\omega) \{ A_{F,\alpha}(x_1, y_1, \omega) \\
& \times A^*_{F,\beta}(x_2, y_2, \omega), \; A_{S,\alpha}(y_1, \omega) B_{S,k}(y_2), \\
& A_{M,\alpha}(y_1, \omega) B_{M,k}(y_2) \}
\end{aligned} \tag{15}$$

$$\begin{aligned}
& {}_5T_{\{F,S,M\},\alpha\beta,kl}(x_1, y_1, t_1; x_2, y_2, t_2; \omega) \\
& = N_\alpha(t_1, \omega) \; {}_2M^*_{kl,\beta}(t_2, \omega) R^*_{l,\beta}(\omega) \\
& \times \{ A_{F,\alpha}(x_1, y_1, \omega) \phi_k(x_1, y_1) \hat{\rho}_1, \; A_{S,\alpha}(y_1, \omega) \hat{B}_{S,k}(y_2), \\
& A_{M,\alpha}(y_1, \omega) \hat{B}_{M,k}(y_2) \}
\end{aligned} \tag{16}$$

$$\begin{aligned}
& {}_4T_{\{F,S,M\},\alpha\beta,jklm}(x_1, y_1, t_1; x_2, y_2, t_2; \omega) \\
& = \hat{M}_{jm,\alpha}(t_1, \omega) \hat{M}^*_{kl,\beta}(t_2, \omega) R_{m,\alpha}(\omega) R^*_{l,\beta}(\omega) \\
& \times \{ \phi_j(x_1, y_1) \phi_k(x_2, y_2), \; B_{S,j}(y_1) B_{S,k}(y_2), \\
& B_{M,j}(y_1) B_{M,k}(y_2) \}
\end{aligned} \tag{17}$$

$$\begin{aligned}
& {}_7T_{\{F,S,M\},\alpha\beta,jklm}(x_1, y_1, t_1; x_2, y_2, t_2; \omega) \\
& = \hat{M}_{jm,\alpha}(t_1, \omega) \; {}_2M^*_{kl,\beta}(t_2, \omega) R_{m,\alpha}(\omega) R^*_{l,\beta}(\omega) \\
& \times \{ \phi_j(x_1, y_1) \phi_k(x_2, y_2) \hat{\rho}_2, \; B_{S,j}(y_1) \hat{B}_{S,k}(y_2), \\
& B_{M,j}(y_1) \hat{B}_{M,k}(y_2) \}
\end{aligned} \tag{18}$$

$$\begin{aligned}
& {}_9T_{\{F,S,M\},\alpha\beta,jklm}(x_1, y_1, t_1; x_2, y_2, t_2; \omega) \\
& = {}_2M_{jm,\alpha}(t_1, \omega) \; {}_2M^*_{kl,\beta}(t_2, \omega) R_{m,\alpha}(\omega) R^*_{l,\beta}(\omega) \\
& \times \{ \phi_j(x_1, y_1) \phi_k(x_2, y_2) \hat{\rho}_1 \hat{\rho}_2, \; \hat{B}_{S,j}(y_1) \hat{B}_{S,k}(y_2), \\
& \hat{B}_{M,j}(y_1) \hat{B}_{M,k}(y_2) \}
\end{aligned} \tag{19}$$

The definitions of used functions are

$$A_{F,\alpha}(x, y, \omega) = e^{(\alpha - i\omega/U)x} \tag{20}$$

$$A_{S,\alpha}(y, \omega) = \iint_{H.A.} e^{(\alpha - i\omega/U)\xi} \, d\xi \, d\eta \tag{21}$$

$$A_{M,\alpha}(y, \omega) = \iint_{H.A.} (\eta - y) e^{(\alpha - i\omega/U)\xi} \, d\xi \, d\eta \tag{22}$$

$$B_{S,j}(y) = \iint_{H.A.} \phi_j(\xi, \eta) \, d\xi \, d\eta \tag{23}$$

$$\hat{B}_{S,j}(y) = \iint_{H.A.} \hat{\rho}(\xi, \eta) \phi_j(\xi, \eta) \, d\xi \, d\eta \tag{24}$$

$$B_{M,j}(y) = \iint_{H.A.} (\eta - y) \phi_j(\xi, \eta) \, d\xi \, d\eta \tag{25}$$

$$\hat{B}_{M,j}(y) = \iint_{H.A.} \hat{\rho}(\xi, \eta) \phi_j(\xi, \eta) (\eta - y) \, d\xi \, d\eta \tag{26}$$

$$N_\alpha(t, \omega) = e^{-\alpha U t} \int_0^t \dot{\psi}(\tau) e^{(\alpha U - i\omega)\tau} \, d\tau \tag{27}$$

$$\hat{M}_{jm,\alpha}(t, \omega) = \int_0^t \phi(\tau) e^{-i\omega\tau} \, {}_2M_{jm,\alpha}(t - \tau, \omega) \, d\tau \tag{28}$$

On the definitions of $R_{m,\alpha}(\omega)$, $M_{jm,\alpha}(t, \omega)$ and ${}_2M_{jm,\alpha}(t, \omega)$, see Ref. 2). The final forms of the geometrical coefficients used in the numerical examples are as follows.

$$\begin{aligned}
A_{S,\alpha}(y, \omega) = & \{ e^{2b(\alpha - i\omega/U)} - 1 \} \{ e^{(\alpha - i\omega/U)(l \sin\Lambda - c_g)} \\
& - e^{(\alpha - i\omega/U)(y \tan\Lambda - c_g)} \} / \{ (\alpha - i\omega/U)^2 \tan\Lambda \} \\
& \qquad \text{for } \alpha - i\omega/U \neq 0 \\
= & \; 2b(l \cos\Lambda - y) \qquad \text{for } \alpha - i\omega/U = 0
\end{aligned} \tag{29}$$

$$A_{M,\alpha}(y,\omega)=\left[e^{2b(\alpha-i\omega/U)}-1\right]\left[e^{(\alpha-i\omega/U)(l\sin\Lambda-c_g)}\right.$$
$$\times\{(l\sin\Lambda-y)/(\alpha-i\omega/U)/\tan\Lambda-1/(\alpha-i\omega/U)^2$$
$$/\tan^2\Lambda\}+e^{(\alpha-i\omega/U)(y\tan\Lambda-c_g)}/(\alpha-i\omega/U)^2$$
$$\left./\tan^2\Lambda\right]/(\alpha-i\omega/U) \qquad \text{for } \alpha-i\omega/U\neq 0$$
$$=b(l\cos\Lambda-y)^2 \qquad \text{for } \alpha-i\omega/U=0 \tag{30}$$

$$B_{S,1}(y)=2b(l\cos\Lambda-y) \tag{31}$$

$$B_{S,2}(y)=B_2 b(l\cos\Lambda-y)(2c_g-2b-l\sin\Lambda-y\tan\Lambda) \tag{32}$$

$$B_{S,3}(y)=\lambda_1\lambda_2\{S_1(e^{-\Lambda_1}-e^{-\Lambda_{1y}}-e^{-\Lambda_3}+e^{-\Lambda_{3y}})$$
$$-S_2(\cos\Lambda_1-\cos\Lambda_{1y}-\cos\Lambda_3+\cos\Lambda_{3y})$$
$$+S_3(\cosh\Lambda_1-\cosh\Lambda_{1y}-\cosh\Lambda_3+\cosh\Lambda_{3y})$$
$$-S_4(\sin\Lambda_1-\sin\Lambda_{1y}-\sin\Lambda_3+\sin\Lambda_{3y})\} \tag{33}$$

$$B_{M,1}(y)=b(l\cos\Lambda-y)^2 \tag{34}$$

$$B_{M,2}(y)=B_2 b(l\cos\Lambda-y)\{c_g\, l\cos\Lambda-c_g\, y$$
$$-\frac{2}{3}l^2\sin\Lambda\cos\Lambda+\frac{1}{3}y^2\tan\Lambda+by$$
$$-bl\cos\Lambda+\frac{1}{3}yl\sin\Lambda\} \tag{35}$$

$$B_{M,3}(y)=\lambda_1\lambda_2[S_1\{e^{-\Lambda_1}(l\cos\Lambda+\lambda_2)-e^{-\Lambda_3}(l\cos\Lambda$$
$$+\lambda_2)-e^{-\Lambda_{1y}}(y+\lambda_2)+e^{-\Lambda_{3y}}(y+\lambda_2)\}$$
$$+S_2\{-l\cos\Lambda\cos\Lambda_1+\lambda_2\sin\Lambda_1+l\cos\Lambda\cos\Lambda_3-\lambda_2\sin\Lambda_3$$
$$+y\cos\Lambda_{1y}-\lambda_2\sin\Lambda_{1y}-y\cos\Lambda_{3y}+\lambda_2\sin\Lambda_{3y}\}$$
$$-S_4\{l\cos\Lambda\sin\Lambda_1+\lambda_2\cos\Lambda_1-l\cos\Lambda\sin\Lambda_3-\lambda_2\cos\Lambda_3$$
$$-y\sin\Lambda_{1y}-\lambda_2\cos\Lambda_{1y}+y\sin\Lambda_{3y}+\lambda_2\cos\Lambda_{3y}\}$$
$$+S_3\{l\cos\Lambda\sinh\Lambda_1-\lambda_2\cosh\Lambda_1-l\cos\Lambda\sinh\Lambda_3+\lambda_2\cosh\Lambda_3$$
$$-y\sinh\Lambda_{1y}+\lambda_2\cosh\Lambda_{1y}+y\sinh\Lambda_{3y}-\lambda_2\cosh\Lambda_{3y}\}]$$
$$-yB_{S,3}(y) \tag{36}$$

where B_2 = normalizing coefficient of pitching mode, S_1, S_2, S_3 and S_4 = normalizing coefficients of bending mode c_g = distance from the front tip of the wing to the center of the gravity, l = wing span, Λ = swept angle. And given constants are;

$\lambda_1=l/\Omega_3/\sin\Lambda$, $\lambda_2=l\cos\Lambda/\Omega_3$,
$\Lambda_1=\{1+(2b-c_g)\sin\Lambda/l\}\Omega_3$, $\Lambda_3=(1-c_g\sin\Lambda/l)$
Ω_3, $\Lambda_{1y}=\{(2b-c_g)\sin\Lambda/l+y/l/\cos\Lambda\}\Omega_3$,
$\Lambda_{3y}=\{y/l/\cos\Lambda-c_g\sin\Lambda/l\}\Omega_3$ and Ω_3=eigen value of the bending vibration.

When $\hat{\rho}$ (x, y) is uniform over the wing, we can equate.

$$\begin{Bmatrix}\hat{B}_{S,j}(y)\\ \hat{B}_{M,j}(y)\end{Bmatrix}=\hat{\rho}_w\begin{Bmatrix}B_{S,j}(y)\\ B_{M,j}(y)\end{Bmatrix} \text{ with } \hat{\rho}_w=\hat{\rho} \tag{37}$$

If the wing has tapered mass distribution or attached mass such as the engine pod, we have to formulate $\hat{B}_{S,j}(y)$ and $\hat{B}_{M,j}(y)$ differently but the the principle remains the same as cited.

Lastly we give the practical forms of $M_{jm,\alpha}(t,\omega)$, $\hat{M}_{jm,\alpha}(t,\omega)$ and $N_\alpha(t,\omega)$ We may have the general expressions for the impulse response functions, Küssner's and Wagner's functions of

$$h_{jm}(t)=\sum_{L=1}^{N_{jm}}C_{jm,L}\,e^{\gamma_L t},\quad \phi(t)=\sum_{\ell_k=1}^{N_k}A_{k,\ell_k}\,e^{a_{k,\ell_k}t}$$

and $\psi(t)=\sum_{\ell_w=1}^{N_w}A_{w,\ell_w}\,e^{a_{w,\ell_w}t}$ respactively. We can compose various sets of $(A_{k,\ell_k}, a_{k,\ell_k})$ and $(A_{w,\ell_w}, a_{w,\ell_w})$ considering the airplane flying speed as far as our calculation is to be based on the strip theory.

Then

$$M_{jm,\alpha}(t,\omega)=\sum_{L}^{N_{jm}}\sum_{\ell_k}^{N_k}C_{jm,L}\,A_{k,\ell_k}\,a_{k,\ell_k}\,I_{L,\ell_k}(t,\omega) \tag{38}$$

$$\hat{M}_{jm,\alpha}(t,\omega)=\sum_{L}^{N_{jm}}\sum_{\ell_k}^{N_k}\sum_{\ell_w}^{N_w}C_{jm,L}\,A_{k,\ell_k}\,A_{w,\ell_w}\,a_{k,\ell_k}$$
$$\times J_{L,\ell_k,\ell_w,\alpha}(t,\omega) \tag{39}$$

$$N_\alpha(t,\omega)=\sum_{\ell_k}^{N_k}A_{k,\ell_k}\,a_{k,\ell_k}\,e^{-\alpha Ut}\,T_0(t,a_{k,\ell_k}+\alpha U-i\omega) \tag{40}$$

where $T_n(t,s)=\int_0^t x^n e^{sx}\,dx$, n = non negative integer. (41)

Depending on the values of γ_L, a_{k,ℓ_k}, α and a_{w,ℓ_w} we have different forms for $I_{L,\ell_k,\alpha}$ and $J_{L,\ell_k,\ell_w,\alpha}$ so we list up six cases;

1) $\alpha U-i\omega+a_{k,\ell_k}=0$ and $\alpha U-i\omega+\gamma_L=0$

$$I_{L,\ell_k,\alpha}(t,\omega)=t^2\,e^{-\alpha Ut/2} \tag{42}$$

$$J_{L,\ell_k,\ell_w,\alpha}(t,\omega)=(G_{00}^2T_2(t,G_{13})/2-2G_{00}T_1(t,G_{13})$$
$$+T_0(t,G_{13}))\,e^{G_{14}t} \tag{43}$$

where $G_{11}=\alpha U-i\omega+a_{k,\ell_k}$, $G_{12}=\alpha U-i\omega+\gamma_L$,
$G_{13}=-\alpha U-a_{w,\ell_w}+i\omega$, $G_{14}=a_{w,\ell_w}-i\omega$.
$G_{00}=\alpha U-i\omega$

2) $G_{11}=0$ and $G_{12}\neq 0$

$$I_{L,\ell_k,a}(t,\omega)=(e^{G_{21}t}-e^{-aUt})/G_{12}^{2}-te^{-aUt}/G_{12} \tag{44}$$

$$J_{L,\ell_k,\ell_w,a}(t,\omega)=\{T_0(t,G_{22})/G_{12}^{2}-G_{00}^{2}T_1(t,G_{13})/G_{12}+(2G_{00}/G_{12}+G_{00}^{2})T_0(t,G_{13})\}e^{G_{14}t} \tag{45}$$

where $G_{21}=\gamma_L-i\omega$, $G_{22}=\gamma_L-a_{w,\ell_w}$.

3) $G_{11}\neq 0$, $G_{12}\neq 0$ and $\gamma_L-a_{w,w}\neq 0$

$$I_{L,\ell_k,a}(t,\omega)=\{(e^{G_{21}t}-e^{G_{32}t})/G_{31}-(e^{G_{21}t}-e^{-aUt})/G_{12}\}/G_{11} \tag{46}$$

$$J_{L,\ell_k,\ell_w,a}(t,\omega)=\{(\gamma_L^{2}/G_{31}-\gamma_L^{2}/G_{12})T_0(t,G_{31})-(a_{k,\ell_k})^{2}T_0(t,G_{33})/G_{31}+G_{00}^{2}T_0(t,G_{13})/G_{12}\}\times e^{G_{14}t}/G_{11} \tag{47}$$

where $G_{31}=\gamma_L-a_{k,\ell_k}$, $G_{32}=a_{k,\ell_k}-i\omega$, $G_{33}=a_{k,\ell_k}-a_{w,\ell_w}$

4) $G_{11}\neq 0$, $G_{12}\neq 0$ and $G_{31}=0$

$$I_{L,\ell_k,a}(t,\omega)=\{te^{G_{32}t}-(e^{G_{21}t}-e^{-aUt})\}/G_{11} \tag{48}$$

$$J_{L,\ell_k,\ell_w,a}(t,\omega)=\{(a_{k,\ell_k})^{2}T_1(t,G_{33})+2a_{k,\ell_k}T_0(t,G_{33})-\gamma_L^{2}T_0(t,G_{22})/G_{12}+G_{00}^{2}T_0(t,G_{13})/G_{12}\}e^{G_{14}t}/G_{11} \tag{49}$$

5) $G_{11}\neq 0$, $G_{12}=0$ and $G_{31}\neq 0$

$$I_{L,\ell_k,a}(t,\omega)=\{(e^{G_{21}t}-e^{G_{32}t})/G_{32}-te^{-aUt}\}/G_{11} \tag{50}$$

$$J_{L,\ell_k,\ell_w,a}(t,\omega)=\{-G_{00}^{2}T_1(t,G_{13})+\gamma_L^{2}T_0(t,G_{22})/G_{31}+2G_{00}T_0(t,G_{13})+(a_{k,\ell_k})^{2}T_0(t,G_{33})/G_{31}\}\times e^{G_{14}t}/G_{11} \tag{51}$$

6) $G_{11}\neq 0$, $G_{12}=0$ and $G_{31}=0$

$$I_{L,\ell_k,a}(t,\omega)=(e^{G_{32}t}-e^{-aUt})t/G_{11} \tag{52}$$

$$J_{L,\ell_k,\ell_w,a}(t,\omega)=\{(a_{k,\ell_k})^{2}T_1(t,G_{33})+2a_{k,\ell_k}T_0(t,G_{33})-G_{00}^{2}T_1(t,-a_{w,\ell w})+2G_{00}T_0(t,-a_{w,\ell_w})\}e^{G_{14}t}/G_{11} \tag{53}$$

NUMERICAL EXAMPLES

The numerical examples are carried out on the same airplane wing configuration as the previous studies[1),2)]. The following physical data were used in the computation: l = 42 ft, b = 7 ft, Λ = 30°, U = 586.6 ft/sec, L_G = 750 ft, ρ_w = 2.5 slugs/ft^2 Ω_3 = 1.955, ω_3 = 13.63 rad/sec.

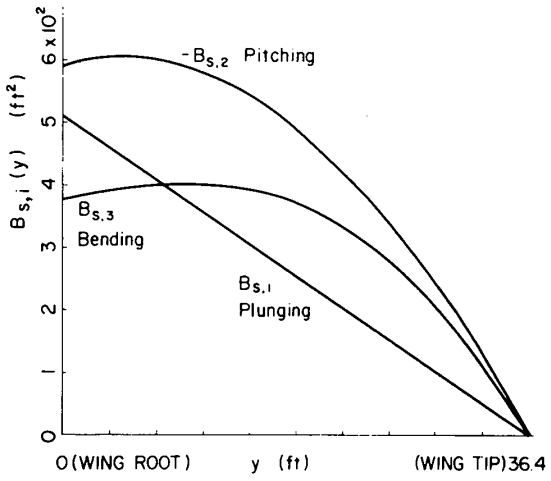

Fig. 2 Spanwise Variation of Shear Coefficients.

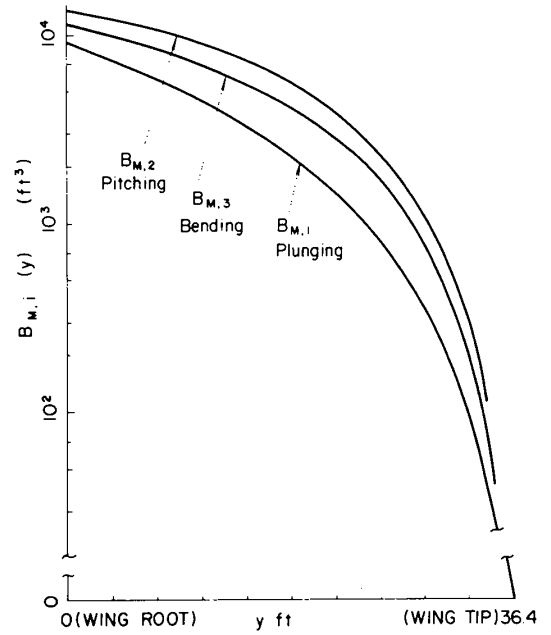

Fig. 3 Spanwise Variation of Moment Coefficients.

The spanwise variation of shear and moment coefficients $B_{S,j}(y)$ and $B_{M,j}(y)$ are given in Fig. 2 and Fig. 3. Those coefficients show the relative weight of the movements to the shear and moment responses. In this example, the absolute value of pitching coefficient is larger than others, which means that the pitching motion contributes most both to the shear and moment responses. The second place of shear coefficients is shared by plunging and bending motions depending on the distance y from the wing root but that of the moment coefficients is occupied by bending vibration for all over the wing span.

Next we give the profile of the envelope function versus retarded time t-x/U in Fig. 4, where the two curves, case A and B, are pictured. In case (A) the gust input reaches the maximum amplitude at about 8 sec. after the airplane enters the turbulence. The result for $t \to \infty$ in case (B) includes the conventional stationary solutions.

The evolutionary spectrum of shear forces at wing root is given by Fig. 5 and Fig. 6 for case (A) and (B) respectively. In both cases, while t is small, the spectrum curves have flat portion below $\omega = 1$ rad/sec and sharp decline in the level for upper frequency range. But as time t gets large, they turn to have double peaks, one at $\omega = 0.1 \sim 1.0$ rad/sec and

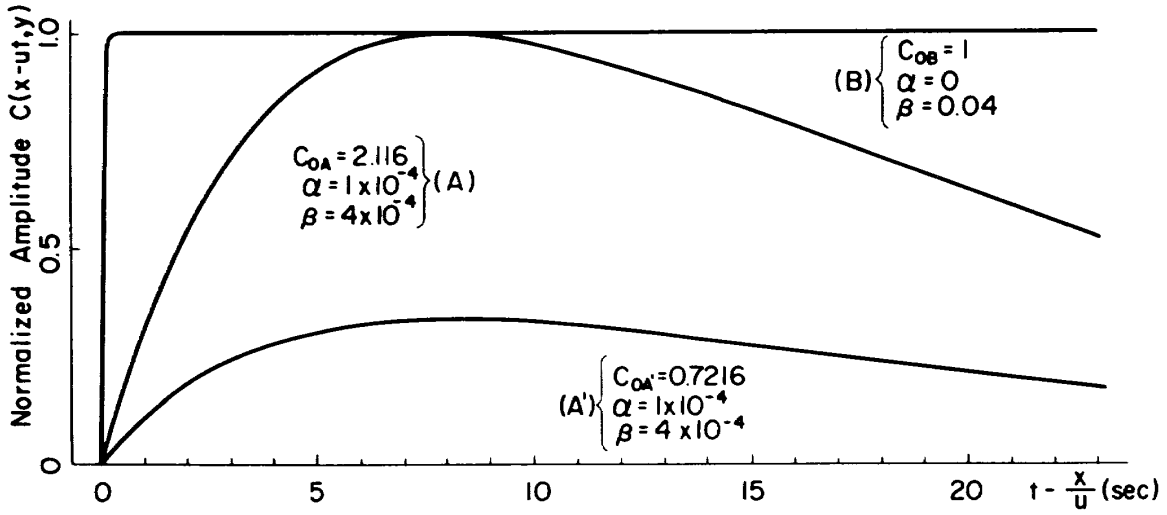

Fig. 4 Profile of the Envelope Function.

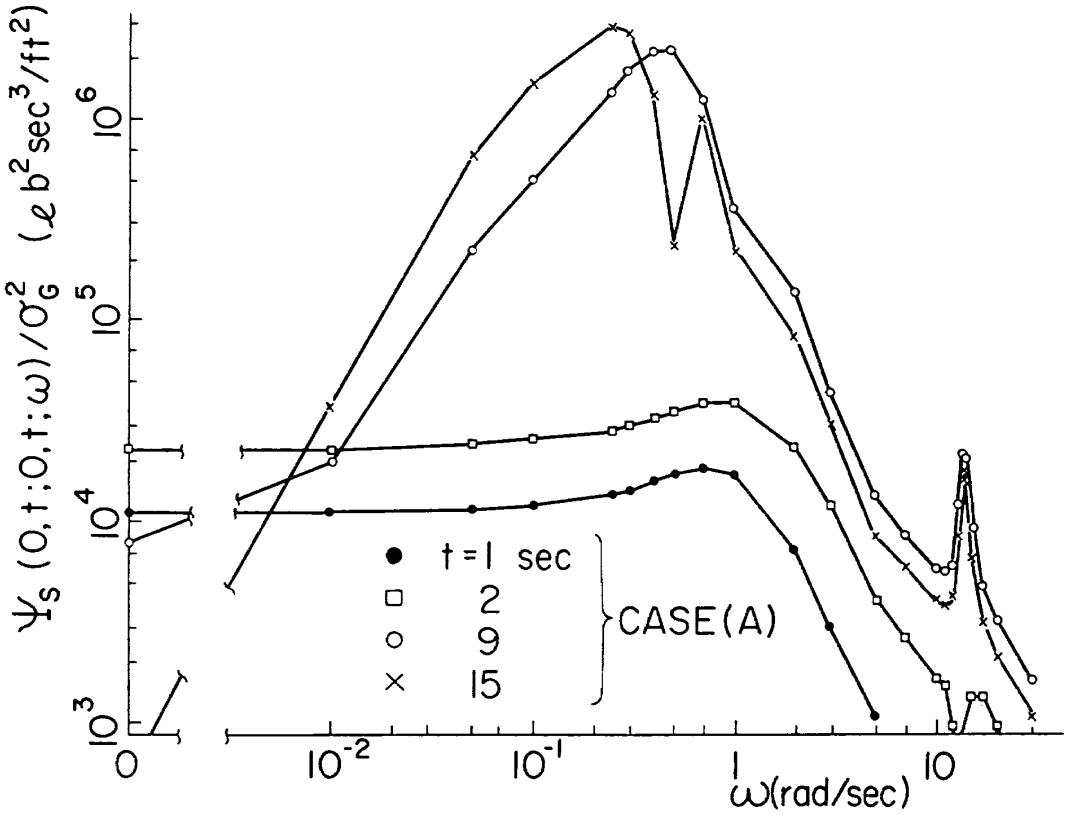

Fig. 5 Evolutionary Spectrum of Shear Forces at the Wing Root for case (A).

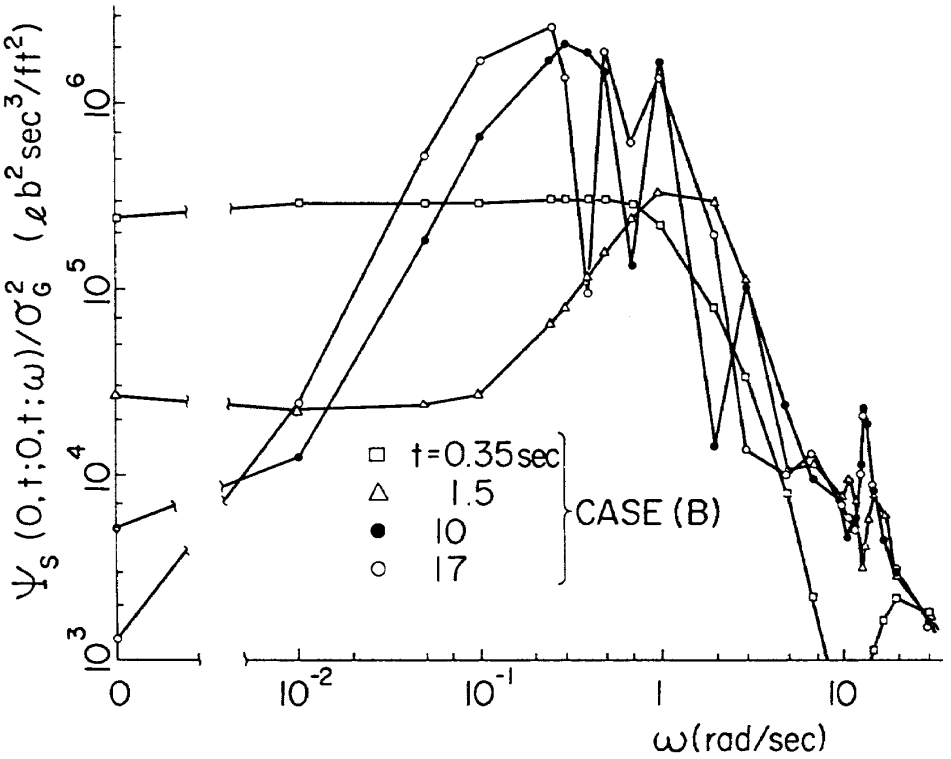

Fig. 6 Evolutionary Spectrum of Shear Forces at the Wing Root for case (B).

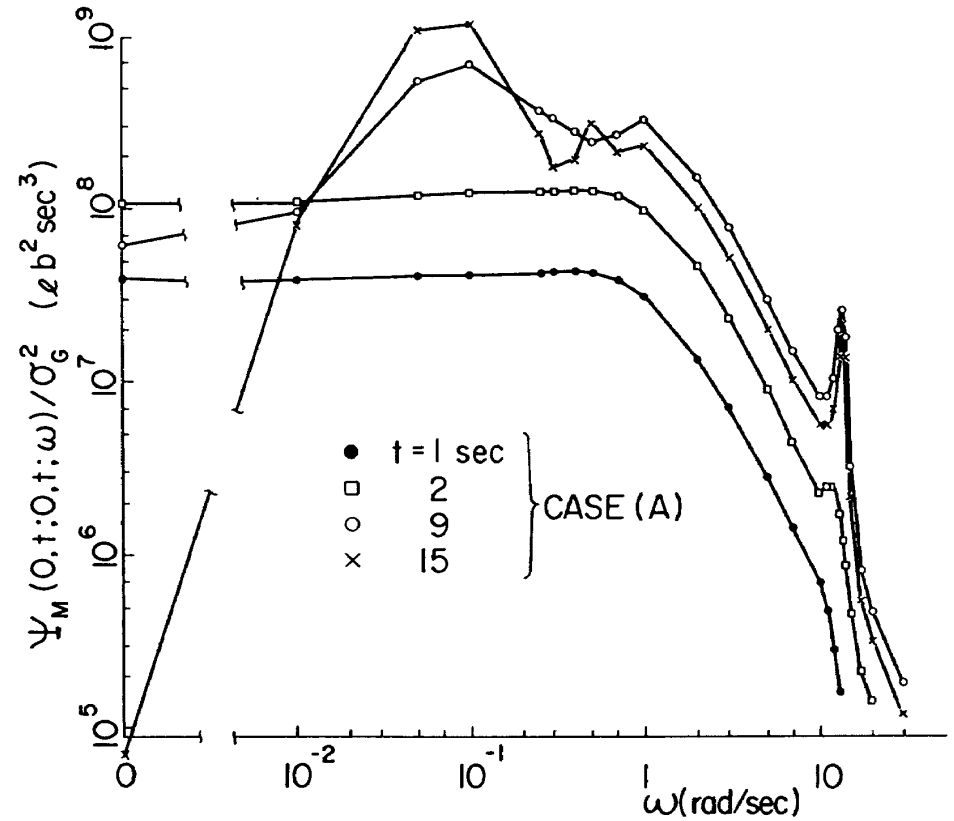

Fig. 7 Evolutionary Spectrum of Moment at the Wing Root for case (A).

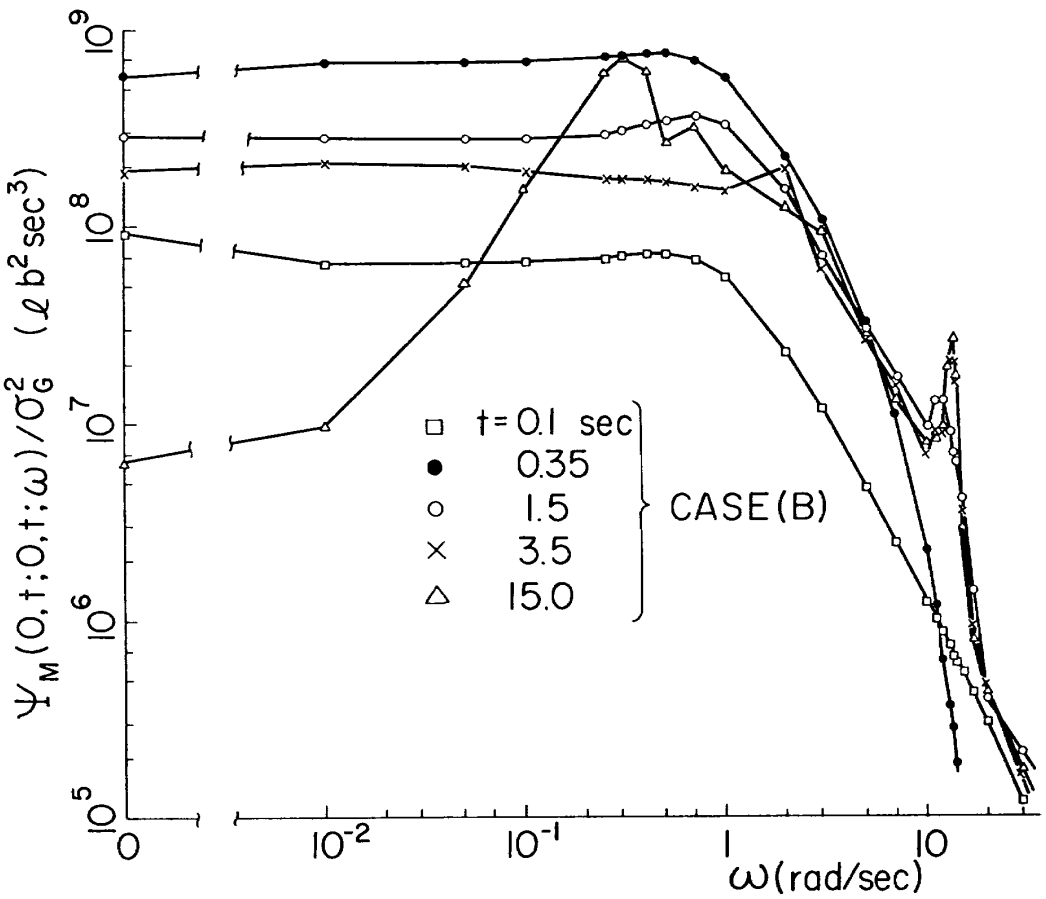

Fig. 8 Evolutionary Spectrum of Moment at the Wing Root for case (B).

the other at ω = 13.6 rad/sec which is the circular natural frequency of the bending vibration. The first peak exhibits the contribution from Dryden's spectrum and the rigid motions. The spectrum curves have some fluctuations in the level at around ω = 0.3 ~ 1.0 rad/sec for large t, so we can do only rough estimate as to where the maximum peak is.

The evolutionary spectrum of moment at wing root is also pictured by Fig. 7 and Fig. 8 for case (A) and (B) respectively. The general profile of curves looks alike to those of the shear force except that the spectrum curves of the bending moment show very stable level all over the frequency considered. Accordingly we can easily detect the maximum level of the spectrum and its corresponding frequency.

Talking on the first peak we have maximum level in the moment and shear spectrum at ω = 0.1 and rad/sec and ω = 0.5 rad/sec respectively when t = 9 sec. in case (A). In case (B) both stationary moment and shear spectrums have the maximum at ω = 0.2 rad/sec. Those values are slightly different from the frequency that makes the Dryden's spectrum maximum, that is, in the present calculation, $\omega = U/L_G/\sqrt{3}$ = 0.451 rad/sec. This shift has risen from the aerodynamic damping effect associated with rigid motions. In either shear or moment spectrum the effect of flexibility comes in at about t = 1.5 sec. Precisely speaking the second peak of the shear spectrum first appears at the upper side of the circular frequency of the first bending vibration, on the contrary that of the moment spectrum does at the lower side and eventually their locations tend to coincide with the first bending frequency.

The mean square value of shear or moment response can be obtained by numerical integration of evolutionary spectrum curves. The time-wise trend of mean square shear in given by Fig. 9 for case (A). The curve takes the maximum at t = 12 sec. which is nearly 4 sec. delayed from the time that makes the envelope function maximum. The mean square

moment of case (A) is graphed in Fig. 10, where we see the same time-wise trend of the curve as that of mean square shear and the maximum occurs at about 9 sec. point. In case (A) roughly speaking the time of maximum moment falls to that of the maximum amplitude given by Fig. 4. The mean square shear for case (B) pictured by Fig. 11 shows quite different time-wise trend from that of Fig. 9, where we observe the maximum at about $t = 12$ sec. and the curve goes, with some fluctuations, to the stable level. The time that makes the mean square shear maximum is almost the same for both cases (A) and (B), which means that the shear response is not sensitive to the envelope profile of the gust field.

Speaking of the mean square shear at the wing root we could say Max. of case (A) > Max. of case

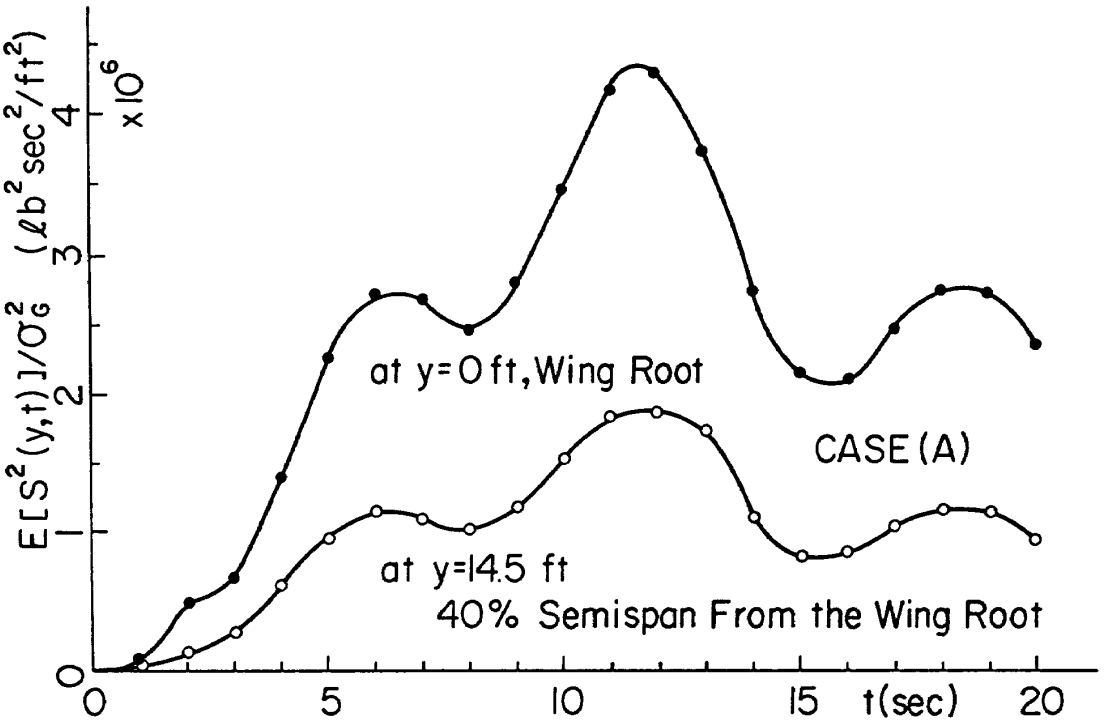

Fig. 9 Mean Square Shear for case (A).

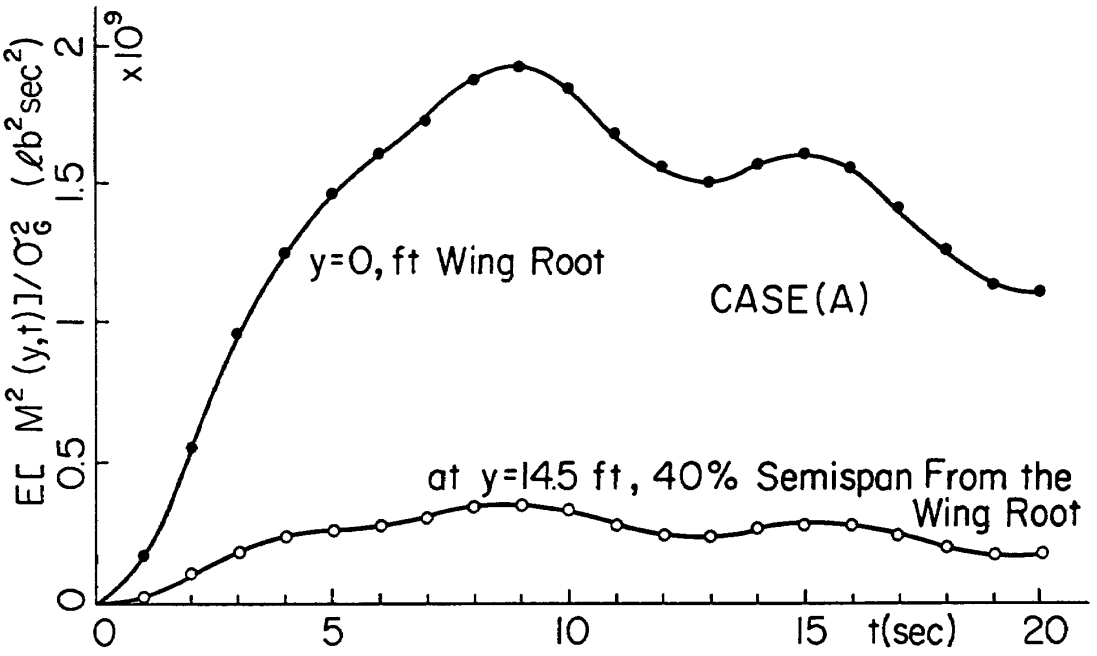

Fig. 10 Mean Square Moment for case (A).

(B) > Stationary level of case (B).

The mean square moment for case (B) is plotted in Fig. 12, where we observe the maximum at about t = 0.35 sec. As we have seen in the evolutionary spectrum curves, at the time of t = 0.35 sec., it is clear that rigid motions dominate. From the level of maximum mean square moment, we can say.

Max. of case (L) > Max. of case (A) ≅ Stationary level of case (B).

The reason that the logarithmic scale is adopted in Fig. 11 and 12 for both response and time is to magnify the incipient stage and stationary level. In practise we need not go further than 4 or 5 sec. to obtain the stationary moment. The results of Fig. 12 for larger time instants are given only for the sake of comparing purposes.

It is meaningful to check the stress levels due to shear force and bending moment. Now the uniform beam of the rectangular cross section with width W and depth H is considered. As we have $\sigma M = MH/2I$ and $\sigma_S = 3S/2WH$ for the maximum stress due to bending moment and that due to shear force respectively, the ratio of mean square values yields

$$\frac{E[\sigma_S^2]}{E[\sigma_M^2]} = \frac{H^2}{16}\,\frac{E[S^2]}{E[M^2]} \tag{54}$$

In case (A) we see from Fig. 9 and 10 that the ratio of the $E[S^2]$ versus $E[M^2]$ is less than 1/100, then taking the root of both sides of Eq. (54) we get

$$\frac{\sqrt{E[\sigma_S^2]}}{\sqrt{E[\sigma_M^2]}} < H \times 7.9 \times 10^{-3} \ll 1, \text{ where H in ft.} \tag{55}$$

Therefore it can be said that stress level due to shear force is negligibly smaller than that due to bending moment. Interaction of shear force and bending moment should be taken into account in the practical structures but the above discussion will not lose its generality. Comparison in terms of strain, strain energy or deflection levels would be different quantitatively but lead to the similar conclusion.

The evolutionary spectrum of shear and moment can be obtained at arbitrary section of the wing. Those results show almost the same frequency distri-

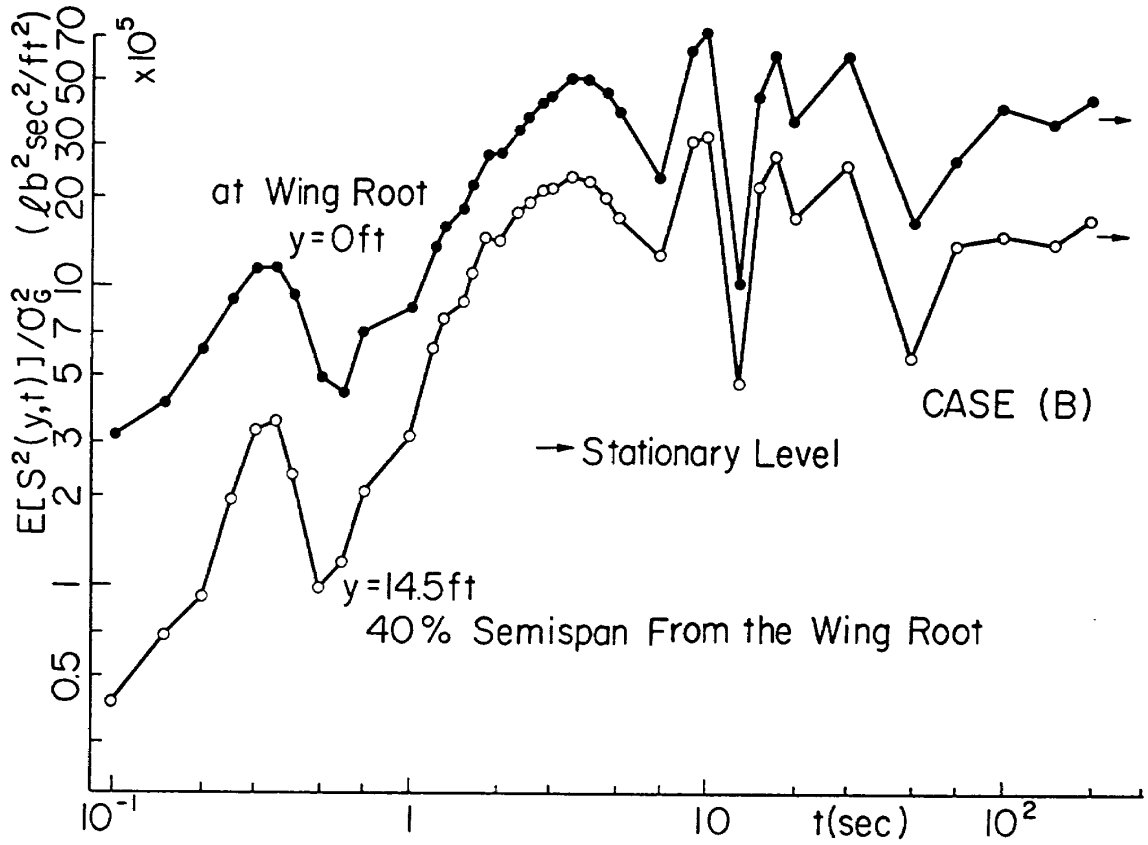

Fig. 11 Mean Square Shear for case (B).

bution as those at the wing root just discussed.

The spanwise variations of the mean square shear and moment are given by Fig. 13 and Fig. 14 for case (A) and (B) respectively. In both cases the results of the moment get gathered almost in one line, and the decrease rate of the values resembles that of moment coefficients in Fig. 3. But the curves of mean square shear scatter much for various time instants and their spanwise decrease rate does not look to have any correlation with the trend of the shear coefficients in Fig. 2.

The evolutionary spectrum Ψ_F or mean square

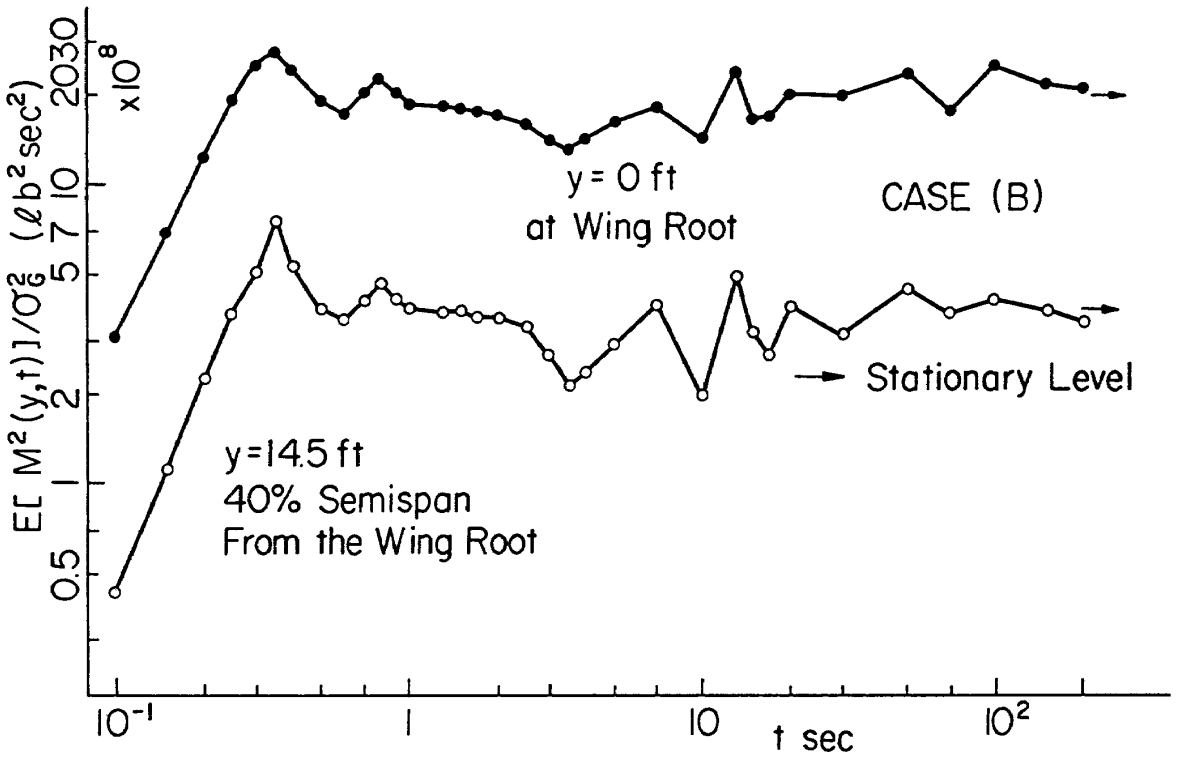

Fig. 12 Mean Square Moment for case (B).

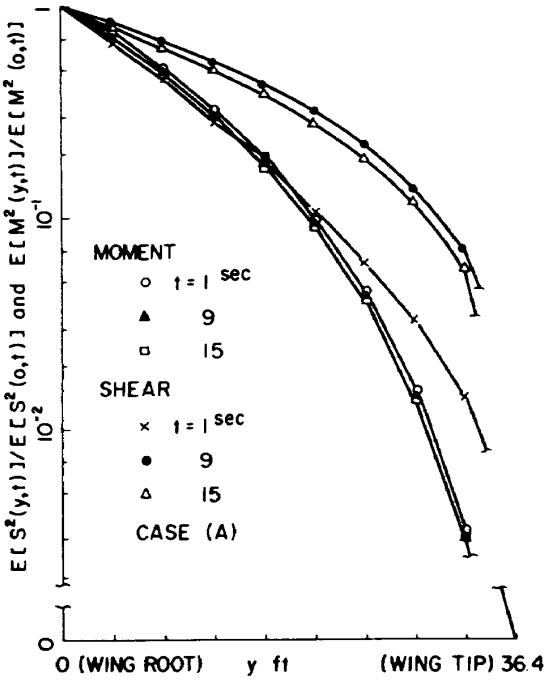

Fig. 13 Spanwise Variation of Mean Square Shear and Moment for case (A).

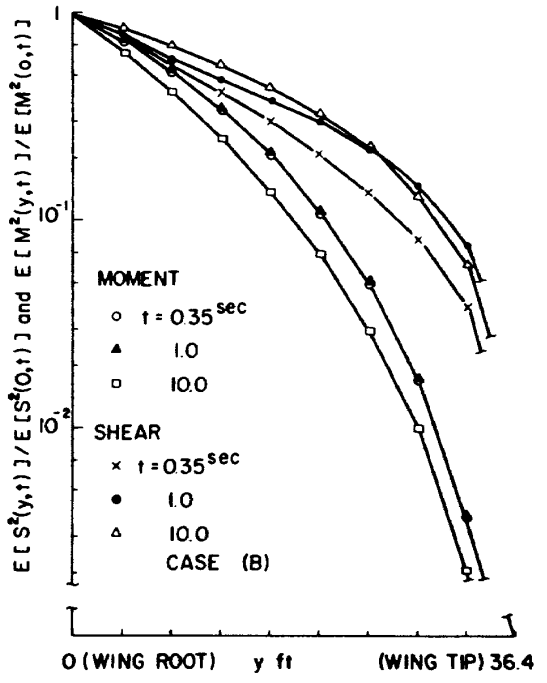

Fig. 14 Spanwise Variation of Mean Square Shear and Moment for case (B).

force per unit area $E[F^2]$ can be obtained in the same manner. Since they are simply the product of the local acceleration and local mass distribution, we did not show the results here. Overall acceleration spectrum or its mean square values already obtained in Ref. 1 suffice for the stress or strain analysis of the airplane structures.

CONCLUDING REMARKS

The general framework to analyze the shear force and the bending moment responses of the airplane wing has been derived based on the evolutionary power spectrum approach.

The contribution by the pitching motion is relatively higher than plunging or bending motions.

The response level due to the shear force in terms of the maximum anticipated stress is negligibly smaller than that due to the bending moment.

Moment response of case (B), where the gust profile looks almost a step function, takes the transient maximum just after entering the gust field. The rigid modes play a predominant role in the evolutionary spectrum at the time of maximum mean square moment. On the other hand, in the evolutionary spectrum at stationary moment, we see the effect of flexibility besides rigid movements.

For the present method to be really useful at the initial design phase of the practical airplane, we should refine the eigen functions of the structure and unsteady aerodynamic force, which can be done by combining the present theory and the existing theories in the related fields.

APPENDIX

It is convenient tha the normalizing constant C_0 of the amplitude profile should be chosen so that the maximum of the curve takes the unit level. In this report the curve (A) of Fig. 4 is used, but in the previous reports[1),2)] the curve of (A′) was taken because of an unduly placed parentheses in the computer program.

In order to compare the spectrums and mean square values of case (A) with those of case (B) it is necessary that the corrective factor $(C_{0A}/C_{0A'})^2 = 8.60$ should be multiplied to the vertical scale of Fig.s 3, 4, 5, 6, 7 and 8 of Ref. 2 and Fig.s 2 and 3 of Ref. 1. Also $C_{0A}/C_{0A'} = 2.93$ to Fig. 4 of Ref. 1. As long as we take the same α and β values, the evolutionary spectrum has the identical frequency distribution, but its level depends on the normalizing constant C_0, so the spectrum of case (A) can be obtained from the relation

$$\Psi_A = \Psi_{A'} (C_{0A}/C_{0A'})^2 .$$

It is recommended that we use the unit maximum for case (A) so that we may compare the response level of case (A) with that of case (B).

REFERENCES

[1] Fujimori, Y. and Lin, Y. K., Analysis of Airplane Response to Nonstationary Turbulence Including Wing Bending Flexibility II, AIAA Journal, Vol. 11, No. 9, September 1973, pp. 1343–1345.

[2] Fujimori, Y. and Lin, Y. K., Analysis of Airplane Response to Nonstationary Turbulence Including Wing Bending Flexibility, AIAA Journal, Vol. 11, No. 3, March 1973, pp. 334–339.

[3] Howell, L. J. and Lin, Y. K., Response of Flight Vehicles to Nonstationary Atmospheric Turbulence, AIAA Journal, Vol. 9, No. 11, November 1971, pp. 2201–2207.

[4] Verdon, J. M. and Steiner, R., Response of a Rigid Aircraft to Nonstationary Atmospheric Turbulence, AIAA Journal, Vol. 11, No. 8, August 1973, pp. 1086–1092.

[5] Houbolt, J. C., Atmospheric Turbulence, AIAA Journal, Vol. 11, No. 4, April 1973, pp. 421–437.

TECHNICAL REPORT OF NATIONAL
AEROSPACE LABORATORY
TR-404T

航空宇宙技術研究所報告404T号(欧文)

昭和50年1月発行

発行所　航空宇宙技術研究所
東京都調布市深大寺町1,880
電話 武蔵野三鷹(0422)47-5911(大代表)
印刷所　株式会社　共進
東京都杉並区久我山4-1-7(羽田ビル)

Published by
NATIONAL AEROSPACE LABORATORY
1,880 Jindaiji, Chōfu, Tokyo
JAPAN